Study on the Dynamic Development of Ground Fissures in Shallow Coal Seam Mining Under Ditch

zheng cheng (20209071011@stu.xust.edu.cn)
Xi'an University of Science and Technology

Research Article

Keywords: Mining under ditch, Ground fissures, VIC-3D system, Dynamic evolution law, The overburden strai

Posted Date: May 28th, 2021

DOI: https://doi.org/10.21203/rs.3.rs-512062/v1

Study on the dynamic development of ground fissures in shallow coal seam mining under ditch

Xueyang Sun[1,2], Zheng Cheng[1], Cheng Li[1,2], Lintian Miao[3]

（1.College of geology and environment, xi 'an university of science and technology, xi 'an 710054, China; 2. Key laboratory of disaster mechanism and prevention and control of mine geological disasters, xi 'an 710054, China; 3. Key laboratory of exploration and comprehensive utilization of coal resources, xi 'an, shaanxi, China）

Abstract

In order to study the dynamic evolution law of ground fissures in shallow coal seam mining under ditch，taking the 14210 working face of a mine in northern Shaanxi as an example, this paper analyzes the dynamic development law of ground fissures in the process of mining under ditch through similar material simulation combined with the VIC-3D monitoring system. The results show that there are 20 ground fissures in the 14210 working face. The development width of ground fissures increases first, then decreases rapidly, and finally closes at the bottom of the ditch. The ground uplifts with a height of 1.5 m. The development width of ground fissures increases first, then decreases slightly, and finally tends to stabilize on the left and the right slopes, resulting in staggered steps with a height of 1.6 m and 0.7 m respectively. This change process is consistent with that of the strain of the underlying overburden obtained by VIC-3D strain analysis. According to their development positions and strain changes, the ground fissures are divided into three categories: tensile ground fissures on the left slope T_1-T_8, squeeze ground fissures at the bottom of the ditch T_9-T_{13}, and tensile ground fissures on the right slope T_{14}-T_{20}. Finally the safety analysis of mining under ditch in the 14210 working face is carried out.

Key words: Mining under ditch. Ground fissures. VIC-3D system. Dynamic evolution law. The overburden strain

Introduction

Ground fissures caused by coal resource mining are the most common geological disasters in mining areas (Howard and Zhou, 2019; Kalogirou et al., 2014), which will cause the lack of water resources and the destruction of surface vegetation and buildings, thus seriously affecting people’s safety and living environment (Bi et al., 2019; Can et al., 2012; Deck et al., 2003; Lamich et al., 2015). The Shenfu mining area is one of the typical shallow coal mining areas in China (Fan et al., 2015). With crisscrossing loess gullies, the ground fissures caused by mining have become a prominent problem (Huang et al., 2019a; Xufeng et al., 2011; Yang et al., 2018b).

Many scholars have carried out research on this problem from different angles. In terms of on-site measurement, Yang et al. (2019) took the Burenta Coal Mine as an example and established an observation station to measure and record the periodic changes of related parameters of ground fissures as the working face advanced, and to explore the topographic deformation laws of shallow coal mining. Through the analysis of the classification of goafs and the distribution characteristics and formation mechanism of ground fissures in Pingyao mining area, Zhou et al. (2011) found that the fissures were non-tectonic, and put forward corresponding prevention and control measures. In terms of physics and computer numerical simulation, through indoor similar simulation experiments, LI et al. (2014) analyzed the spatio-temporal evolution of overburden fissures during coal mining from qualitative and quantitative perspectives. Yang et al. (2018a) presented the mechanical model of "cantilever beam and elastic foundation beam" through two physical simulation experiments, calculated the stress distribution and crack initiation angle of the overlying strata， and well explained the mechanism of

ground fissure generation and expansion. Zhao et al. (2016) used FLAC3D software to simulate coal seam mining, calculated the displacement and tensile strain of the ground and the stratum, and predicted the distribution of ground fissures. In addition, some scholars conducted related theoretical analysis and numerical calculations. Liu et al. (2019), taking the Daliuta coal mine in the Shendong mining area of China as an example, introduced a new comprehensive influencing parameter K of geology and mining on the development of ground fissures to explain the impact of mining speed on the development characteristics of ground fissures. Huang et al. (2019) proposed the relationship between the development speed of ground fissures caused by mining and the scope of the damaged area, and put forward effective measures to control the development of boundary fissures. Li and Liu (2019) explored the dynamic changes of ground fissures in shallow coal seam mining by studying the spatial-temporal distribution of overlying rock fissures and gas conductivity. Álvarez-Fernández et al. (2005); Díaz-Fernández et al. (2010); Díez and Álvarez (2000) succeeded in proposing a three-dimensional development of n-k-g impact function to make the prediction of ground subsidence and fissures possible. To sum up, most scholars have done more research on the dynamic development and evolution of ground fissures in shallow coal seams, but less on the dynamic development of ground fissures in shallow coal seam mining under ditch in gully areas.

This paper applies similar material simulation combined with the VIC-3D monitoring system to study the dynamic development of ground fissures in the 14210 working face of a mine in northern Shaanxi and analyzes the safety of ground fissures. Obtaining the development law of ground fissures in valley coal seam mining and putting forward effective measures to prevent the water from flowing into the working face, this article provides a reference for the prevention of ground fissures in shallow coal seam mining under ditch.

Basic situation of the working face

Geological condition of the working face

The 14210 working face is located in the middle of a mine in the north of Shaanxi, which is a blown-sand area. The strike of the working face is north-south, making an angle of approximately 60° with the perennial Ulanbula Ditch. The thickness of the coal seam is 2.87-3.92 m in the working face, and the average thickness is 3.57 m, with 1-3 layers of gangue, the thickness of which is 0.2-0.55 m. When the working face passes the ditch, the 4-2 coal is nearly 3 m thick covered by about 16.65-m-thick fresh bedrock and about 5.1-m-thick weathered bedrock with an overlying loose sandy soil layer of 1.2-2.5 m.

The thickness of fresh bedrock on the roof of 4-2 coal seam is 16.65-51 m, and the thickest part falls in the north of the working face. The fresh bedrock is only 16.65 m thick under the ditch and covered by weathered bedrock or 3-1 burnt rock, with an overlying loose layer of 0-80 m.

Mining situation of the working face

The working face, with a strike length of 3400 m and a trend of about 300 m, contains three channels：the rubber transport channel, the auxiliary transport channel and the return air channel. Adopting fully-mechanized method and mining 4-2 coal, the working face has a designed production capacity of 5.07 Mt/a. Natural caving method is adopted in roof management. The elevation of the working face floor ranges from 1100 m to 1130 m. To the east is the 14209 working face, to the west the 14214 working face, and to the southeast the coal seam outcrop line and the fire boundary line.

Similar material simulation experiment

In this experiment, the 14210 working face of the mine is taken as the research object, and mining 4-2 coal is simulated. The average thickness of the 4-2 coal under the ditch is 3 m, covered by 16.65-m-thick fresh bedrock and 5.1-m-thick weathered bedrock. On the weathered bedrock is a loose sandy soil layer with a thickness of 1.2-2.5 m. The thickness and physical and mechanical parameters of coal and rock are shown in Table 1. In order to meet the similarity requirements of similar materials and natural rocks, river sand is selected as the aggregate for the model, gypsum and white powder in different proportions as the cementing material, to simulate soft and hard rock formations. In addition, mica powder is used to simulate the layer and interlayer bedding surface. This experiment uses the ratio of soil: sand: oil=4.5:4.5:1 to better simulate the mechanical properties of the overlying red soil layer (Cheng et al., 2016; Zhang et al., 2020). The geometric size of the experimental model is 4000 mm×1010 mm×200 mm (length×height×width), and the geometric similarity ratio is 1:100, as shown in Fig. 1. With a step of 10 m and a mining height of 3.7 m, the simulated working face is excavated from left to right for 34 times and advances 340 m, in order to observe the dynamic development of ground fissures during ditch mining.

The experiment uses the VIC-3D monitoring system (non-contact full-field strain measurement system) to measure the surface deformation of the model (Strungar et al., 2019). By capturing the movement of speckle features at the pixel level, it provides the morphological appearance, displacement and strain data measurement in two-dimensional and three-dimensional space (Pazmino et al., 2014; Tang et al., 2010). The VIC-3D monitoring system is widely used in the fracture process of defective materials and some civil engineering experiments (Caduff and Van Mier, 2010; Kopanitsa et al., 2018a; Kopanitsa et al., 2018b).

Table 1 Physical and mechanical parameters of coal rocks

Strata	Thickness/ m	Density / kg/m^3	Bulk modulus/ Pa	Cohesion/ Pa	Internal friction angle (°)	Tensile strength/ Pa
Aeolian sand	6.97	2 183	2.62E+08	0.00E+00	35	0.00E+00
Red clay	5	2 560	1.21E+08	2.00E+04	31	1.00E+03
Mudstone	2	2 750	6.21E+09	8.00E+05	15	1.50E+05
Fine-grained sandstone	9.7	2 750	6.21E+09	8.00E+05	15	1.50E+05
Siltstone	2.4	2 700	6.21E+09	2.50E+06	38.13	8.70E+05
Fine-grained sandstone	2.44	2 630	5.67E+09	2.40E+06	38.65	8.70E+05
Siltstone	1.3	2 730	6.21E+09	2.50E+06	38.13	8.70E+05
Fine-grained sandstone	6.76	1 390	1.80E+08	1.20E+06	39.11	2.20E+05
3-1 coal	2.62	2 650	6.21E+09	2.11E+06	38.8	7.80E+05
Fine-grained sandstone	4.28	2 490	8.37E+09	3.66E+06	38.69	6.50E+05
Mudstone	9.5	2 650	6.21E+09	2.11E+06	38.8	7.80E+05
Siltstone	23	2 680	5.67E+09	3.13E+06	39.3	1.75E+06
Siltstone	3	1 380	1.80E+08	1.16E+06	37	2.40E+05
4-2 coal	3.7	2 760	5.82E+09	3.66E+06	37.5	1.09E+06
Fine-grained sandstone	5.1	2 720	6.21E+09	2.64E+06	40.4	1.24E+06
Siltstone	15.45	2 730	6.21E+09	2.50E+06	38.13	8.70E+05

Lithology	Layer thickness /m
Aeolian sand	7
Red clay	5
Mudstone	2
Fine-grained sandstone	10
Siltstone	2
Fine-grained sandstone	2
Siltstone	1
Fine-grained sandstone	7
3-1 coal	3
Fine-grained sandstone	4
Mudstone	10
Siltstone	23
Siltstone	3
4-2 coal	4
Fine-grained sandstone	2

Fig.1 Experimental model

4-2 development law of coal ground fissures

Similar material simulation displays that 20 ground fissures are developed in the experiment, denoted as T_1 to T_{20}. Among them, 8 ground fissures are on the left slope of the ditch, the spacing of which is 12 m, 8 m, 13 m, 14 m, 28 m, 6 m, and 9 m respectively. 5 ground fissures are developed at the bottom of the ditch, the spacing of which is 7 m, 8 m, 6 m, and 8 m respectively, and 7 ground fissures are developed on the right slope, the spacing of which is 12 m, 8 m, 27 m, 12 m, 11 m, and 12 m (Fig. 6). It can be seen from Fig. 2a that ground fissures are approximately symmetrical on the left and the right slopes, and the fissure spacing is small at the bottom of the ditch.

With the continuous advancement of the working face, the ground fissures will produce different dynamic changes. At the bottom of the ditch, the development width of T_{10} fissures first increases, then rapidly decreases, and finally closes (Fig. 2a). Moreover, the ground is uplifted by the compressive stress with a height of 1.5 m (Fig. 2b). The development width of T_4 ground fissures on the left slope increases first, then decreases, and finally stabilizes at 0.8 m. Meanwhile, a step-shaped ground fissure is formed with a height of 1.6 m. (Fig. 2c). The development width of T_{17} ground fissure first increases and then decreases on the right slope, and stabilizes at 0.2 m after the mining is completed. A staggered ground fissure opposite to the left slope is formed on the ground surface, with a height of 0.7m (Fig. 2d).

Through the longitudinal comparison of the fissures on the left slope, at the bottom, and on the right slope, it is found that mining downhill generates forward step-shaped fissures, and mining downhill generates reverse step-shaped fissures, the latter distinctly outnumbering the former. There are fewer ground fissures at the bottom of the trench than on the slope, which have smaller spacing.

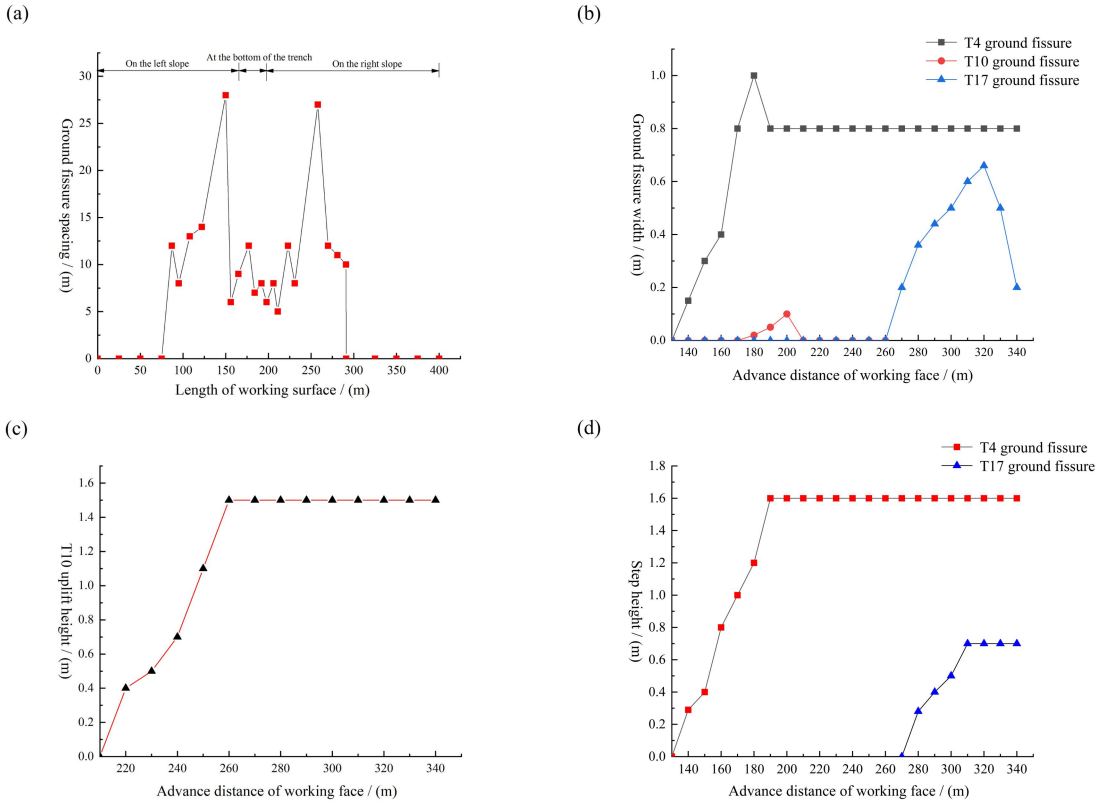

Fig.2 Dynamic development process of ground fissures : **a** distribution map of ground fissure spacing b, **b** dynamic width of ground fissure, **c** T_{10} uplift height chart, **d** T_4 and T_{17} step height

Strain analysis of overlying rock based on VIC-3D system

Strain analysis of ground fissures at the bottom of ditch

In the process of coal mining, due to the influence of mining disturbance, the upper overlying rock collapses and produces fissures. With the continuous advancement of the working face, the fissures continue to develop upward into ground fissures, which will have different changes. The following Fig3 shows the strain process of the rock mass under the T_{10} ground fissure when the coal seam is excavated to 180 m, 200 m, and 220 m. When the coal seam is excavated to 180 m, the coal seam mining position moves to the left of the bottom of the ditch, the width of the fissure increases due to the tensile stress from the overburden. At this point, the strain value of the overburden under T_{10} is 0.064 (Fig. 3a). When the coal seam is excavated to 200 m, the coal seam mining position is at the bottom of the ditch, where the influence of tensile stress becomes greater. The width of the ground fissure reaches the maximum, and the strain value of the overburden under T_{10} increases to 0.065 (Fig. 3b). When the coal seam is excavated to 220 m, the coal seam mining position is on the right side of the bottom of the ditch. After the working face passes the ditch, the tensile stress disappears and the compressive stress increases, and the strain value of the underlying overburden decreases to 0.056 (Fig. 3c). Then as the working face continues to advance, the coal seam excavation position is further away from T_{10}, the compressive stress further increases, and the strain value of the underlying overburden decreases.

It can be obtained that before the working face passes the ditch, the ground fissure is subjected to tensile stress. As the strain of the underlying overburden increases, the width of the ground fissure also increases, and reaches the maximum when the working face passes through the bottom of the ditch. After the working face passes the ditch, the fissure is under compressive stress, the strain of the

overburden decreases, and the ground fissure first closes and then uplifts (Fig. 3 d).

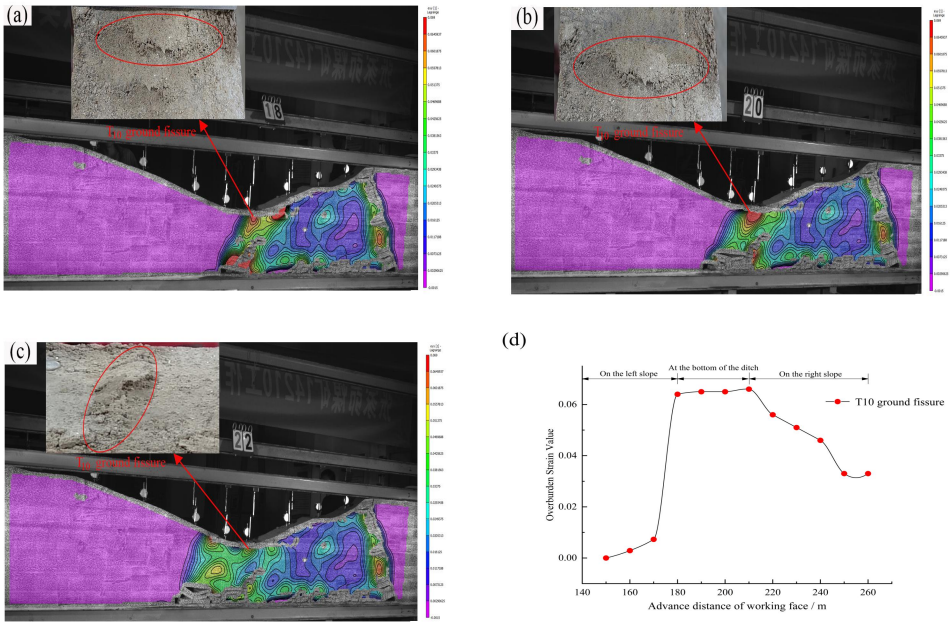

Fig. 3 T_{10} ground fissure shape and underlying overburden strain : **a** working face advancing 180 m , **b** working face advancing 200 m , **c** working face advancing 220 m , **d** underlying overburden strain

Analysis of ground fissure strain on the left slope (downslope direction)

Fig. 4 shows the strain development process of the ground fissure T_4 on the left slope when the coal seam is excavated to 160 m, 180 m and 200 m. When the working face advances to 160 m, the overburden under the T_4 ground fissure begins to deform due to tensile stress, with a strain value of 0.014 (Fig. 4a), forming positive staggered steps. When the working face advances to 180 m, the reduction of coal wall support stress leads to a continuous increase in tensile stress, and the strain value increases to 0.064 (Fig. 4b). When the working face advances to 200 m, the goaf is compacted and the strain stabilizes at 0.012 (Fig. 4c).

It can be concluded that the strain of the overburden under the ground fissure on the left slope first increases and then decreases. The corresponding development process of ground fissures is that the width first increases and then decreases, forming larger scattered steps, and finally stabilizes (Fig. 4d).

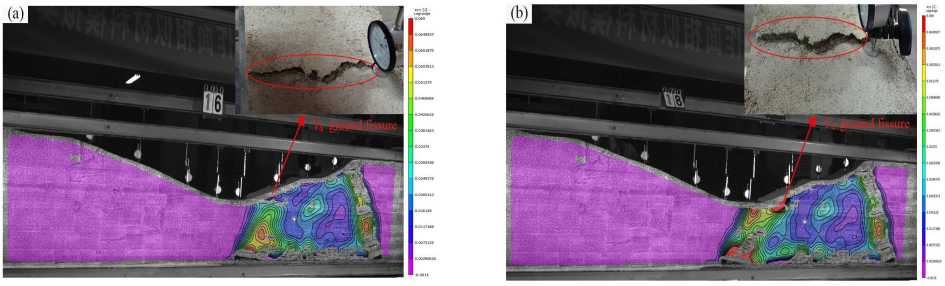

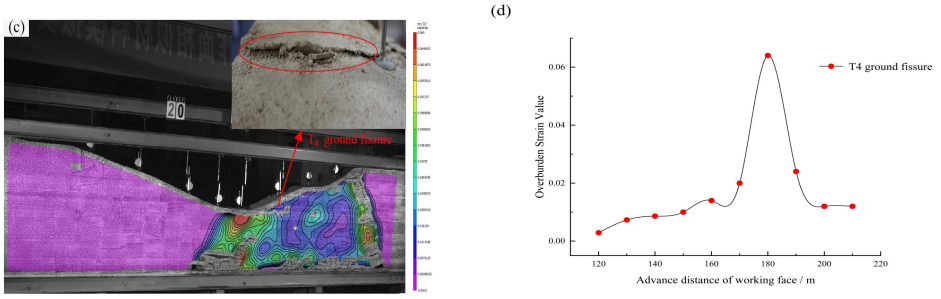

Fig. 4 T_4 ground fissure shape and underlying overburden strain : **a** working face advancing 160 m , **b** working face advancing 180 m , **c** working face advancing 200 m , **d** underlying overburden strain

Analysis of ground fissure strain on the right slope (upslope direction)

Fig. 5 shows the strain development process of the ground fissure T_{17} on the right slope when the coal seam is excavated to 270 m, 290 m and 310 m. When the working face advances to 270 m, the overburden under the T_{17} ground fissure is deformed due to severe tensile stress, with a strain value of 0.064, and staggered steps are formed on the surface opposite to the left side slope (Fig. 5a). When the working face advances to 290 m, the coal seam is mined through the T_{17} ground fissure, the tensile stress of the overburden under the T_{17} ground fissure decreases, and the strain begins to decrease to 0.042 (Fig. 5b). When the working face advances to 310 m, the coal seam has been fully mined at this point, and the strain value of the overburden under the fissure stabilizes at 0.040 (Fig. 5c).

It can be concluded that the strain of the overburden under the ground fissure on the right slope first increases, then decreases, and finally reaches a stable state. The corresponding development process is that the width of ground fissures first increases, then decreases and finally stabilizes, forming scattered steps (Fig. 5d).

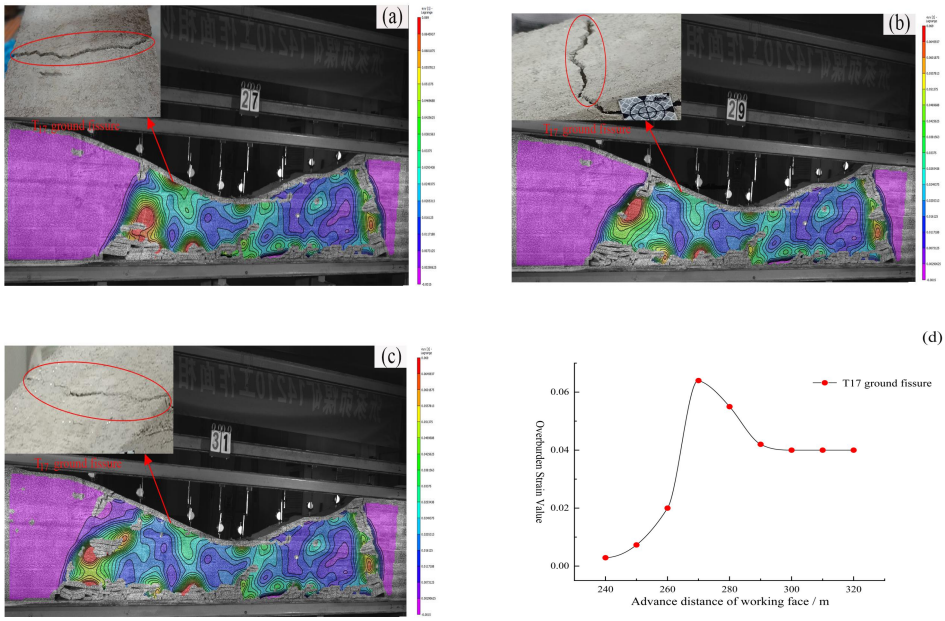

Fig. 5 T_{17} strain variation process of the underlying overburden : **a** working face advancing 270 m , **b** working face advancing 290 m , **c** working face advancing 310 m , **d** underlying overburden strain

Classification of ground fissures

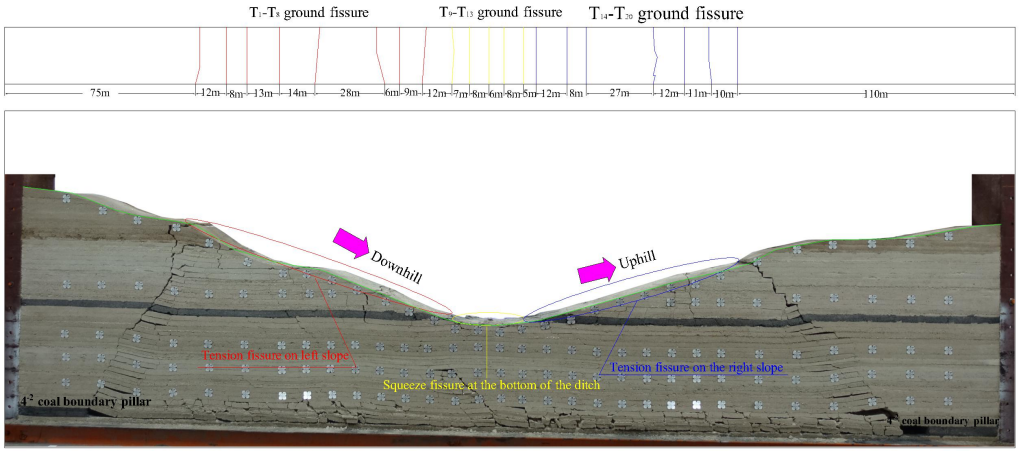

Fig. 6 Ground fissures partition diagram

According to the results of similar material simulation and the analysis results of the VIC-3D monitoring system, the T_1-T_{20} ground fissures can be divided into 3 categories, as shown in Fig. 6. They are tensile ground fissures on the left slope T_1-T_8, squeeze ground fissures at the bottom of the ditch T_9-T_{13}, and tensile ground fissures on the right slope T_{14}-T_{20}. Based on the above analysis, although the ground fissures on the left and the right slopes of the model are both tensile fissures, due to insufficient mining on the left slope, both the width of the fissures and the height of the staggered platforms there are larger than those on right side slope, which causes severe damage to the surface of the earth. At the bottom of the ditch, ground fissures are generated by compressive stress, which leads to the closure and uplift of ground fissures.

Discussion and conclusion

Safety analysis

Based on mining experience under similar conditions and existing research results, combined with actual mining geological conditions, the safety analysis of mining under ditch in the 14210 working face is carried out. The development width of ground fissures is large on the left and right slopes, especially the permanent ground fissures formed at the opening cut and the stop mining line. In addition, precipitation and groundwater will promote the development of ground fissures, and surface water will enter the working face along the slope where the ground fissures are wider. The density of ground fissures is small at the bottom of the ditch, and with the advancement of the working face, the ground fissures undergo a change from tensile stress to compressive stress, and eventually tend to close. However, the ground fissures on the slope are under tensile stress, which widens the ground fissures, and water is more easily conducted on the slope. The water level in the ditch will also directly affect the safety of the working face. In the dry season, the water level does not rise to the slope surface and will not have a major impact on the mining of the working face. However, in the wet season, the water level will rise, and water will enter the working face along the tensile ground fissures on the slope, affecting the safety of the mine. In addition, dynamic ground fissures always develop before the working face is mined, so there is a certain linear relationship between the advancing speed of the working face and the development of ground fissures.

In summary, during the ditch mining period, there are four factors for the influx of water in Ulanbula Ditch into the working face, which are the width of fissures, the distribution density of fissures, the water level in the ditch, and the advancing speed of the working face.

In view of the above factors, with the precondition of guaranteed quality of the project, detraction

mining can be used in the advancement of the working face. By setting up coal pillars, the high stress of the overlying rock under mining can be relieved, and the coupled control of uniform surface settlement and the development of ground fissures can be realized (Huang et al., 2019b). At the same time, backfill materials such as coal stone, fly ash, ordinary Portland cement and ultra-high water materials can be used for backfilling, which effectively controls the formation and development of ground fissures (LEI et al., 2014; Zhu et al., 2018b). At the opening cut and the stop mining line, the permanent ground fissures can be repaired to prevent surface water from entering (Zhu et al., 2018a). The advancing speed of the working face should be accelerated in the dry season and reduced in the wet season. Since there is water all year round at the bottom of the ditch，the advancement should slow down (Zhang et al., 2011). Meanwhile, grouting can be used to consolidate the overlying loose sand, increase the thickness of the bedrock, and weaken the development of the water channel.

Conclusion

This paper takes the 14210 working face of a mine in northern Shaanxi as the research object and conducts a similar material simulation by using VIC-3D detection method. With the advancement of the working face, the dynamic evolution law of ground fissures is obtained, and the safety analysis of ground fissures is carried out. The main conclusions are as follows:

1. The dynamic development process of ground fissures in shallow coal seam mining under ditch is obtained by means of similar material simulation. At the bottom of the ditch, the development width of the fissures first increases and then decreases rapidly, and finally closes and produces a ground uplift. On the left and the right slopes, the development width of ground fissures increases first and then stabilizes, resulting in staggered steps.

2. From the analysis of the overlying rock strain of the model through the VIC-3D system, it can be seen that at the bottom of the ditch, the strain first increases and then decreases, the stress changes from tension to compression, and the ground fissures uplift. On both the left and the right slopes, the strain first increases and then decreases slightly, which is caused by tension. The fissures display a form of steps. All this is consistent with the phenomenon observed by simulation of similar materials.

3. 4-2 coal mining results in a total of 20 ground fissures. According to their locations and strain changes, they can be roughly divided into three categories: tensile ground fissures on the left slope, squeeze ground fissures at the bottom of the ditch, and tensile ground fissures on right slope.

4. The safety analysis of mining under ditch in the 14210 working face is carried out. During the ditch mining period, there are 4 factors that will cause Ulanbula Ditch spring water to pour into the working face, which are the width of the ground fissures, the distribution density of the ground fissures, the water level in the ditch, and the advancing speed of the working face.

References

Álvarez-Fernández MI, González-Nicieza C, Menéndez-Díaz A, Álvarez-Vigil AE (2005) Generalization of the n–k influence function to predict mining subsidence. Engineering Geology 80:1-36. doi:https://doi.org/10.1016/j.enggeo.2005.02.004

Bi Y, Zhang J, Song Z, Wang Z, Qiu L, Hu J, Gong Y (2019) Arbuscular mycorrhizal fungi alleviate root damage stress induced by simulated coal mining subsidence ground fissures. Science of The Total Environment 652:398-405. doi:https://doi.org/10.1016/j.scitotenv.2018.10.249

Caduff D, Van Mier JGM (2010) Analysis of compressive fracture of three different concretes by means of 3D-digital image correlation and vacuum impregnation. Cement and Concrete Composites 32:281-290. doi:https://doi.org/10.1016/j.cemconcomp.2010.01.003

Can E, Kuşcu Ş, Mekik C (2012) Determination of underground mining induced displacements using GPS observations in Zonguldak-Kozlu Hard Coal Basin. International Journal of Coal Geology 89:62-69. doi:https://doi.org/10.1016/j.coal.2011.08.006

Cheng W, Sun L, Wang G, Du W, Qu H (2016) Experimental research on coal seam similar material proportion and its application. International Journal of Mining Science and Technology 26:913-918.

Deck O, Al Heib M, Homand F (2003) Taking the soil–structure interaction into account in assessing the loading of a structure in a mining subsidence area. Engineering Structures 25:435-448. doi:https://doi.org/10.1016/S0141-0296(02)00184-0

Díaz-Fernández ME, Álvarez-Fernández MI, Álvarez-Vigil AE (2010) Computation of influence functions for automatic mining subsidence prediction. Computational Geosciences 14:83-103. doi:10.1007/s10596-009-9134-1

Díez RR, Álvarez JT (2000) Hypothesis of the multiple subsidence trough related to very steep and vertical coal seams and its prediction through profile functions. Geotechnical & Geological Engineering 18:289-311. doi:10.1023/A:1016650120053

Fan L, Zhang X, Xiang M, Zhang H, Shen T, Lin P (2015) Characteristics of ground fissure development in high intensity mining area of shallow seam in Yushenfu coal field. China Coal Soc 40:1442-1447.

Howard KW, Zhou W (2019) Overview of ground fissure research in China. Environmental Earth Sciences 78:97.

Huang Q, He Y, Cao J (2019a) Experimental Investigation on Crack Development Characteristics in Shallow Coal Seam Mining in China. Energies (19961073) 12:1302-1302. doi:10.3390/en12071302

Huang Q, He Y, Cao JJE (2019b) Experimental investigation on crack development characteristics in shallow coal seam mining in China. 12:1302.

Kalogirou EE, Tsapanos TM, Karakostas VG, Marinos VP, Chatzipetros A (2014) Ground fissures in the area of Mavropigi Village (N. Greece): Seismotectonics or mining activity? Acta Geophysica 62:1387-1412.

Kopanitsa D, Ustinov A, Potekaev A, Klopotov A, Marchenko EJRPJ (2018a) Changes in the Stress¨CStrain States of Subsurface Layers of Steel During Loading. 60:1577-1585.

Kopanitsa DG, Ustinov AM, Potekaev AI, Klopotov AA, Marchenko ES (2018b) Changes in the Stress–Strain States of Subsurface Layers of Steel During Loading. Russian Physics Journal 60:1577-1585. doi:10.1007/s11182-018-1254-4

Lamich D, Marschalko M, Yilmaz I, Bednářová P, Niemiec D, Kubečka K, Mikulenka V (2015) Subsidence measurements in roads and implementation in land use plan optimisation in areas affected by deep coal mining. Environmental Earth Sciences 75:69. doi:10.1007/s12665-015-4933-2

LEI S-G, DENG K-Z, WANG Y-X (2014) Research on ground fissure treatment filling with super-high-water material. Journal of China Coal Society 39:72-77.

LI H-Y, WANG W-H, JI Q-X, ZHANG L (2014) Study on fissure development rule of overlying strata influenced by mining based on fractal theory. Journal of China Coal Society 39:1023-1030.

Li J, Liu C (2019) Spatio-temporal distribution and gas conductivity of overburden fissures in the mining of shallow thick coal seams. European Journal of Environmental and Civil Engineering 23:1019-1033.

Liu H, Deng K, Zhu X, Jiang C (2019) Effects of mining speed on the developmental features of mining-induced ground fissures. Bulletin of Engineering Geology and the Environment 78:6297-6309.

Pazmino J, Carvelli V, Lomov SV, Van Mieghem B, Lava PJIjomf (2014) 3D digital image correlation

measurements during shaping of a non-crimp 3D orthogonal woven E-glass reinforcement. 7:439-446.
Strungar E, Yankin A, Zubova E, Babushkin A, Dushko AJAMS (2019) Experimental study of shear properties of 3D woven composite using digital image correlation and acoustic emission.1-12.
Tang Z-Z, Liang J, Xiao Z-Z, Guo C, Hu HJOE (2010) Three-dimensional digital image correlation system for deformation measurement in experimental mechanics. 49:103601.
Xufeng W, Dongsheng Z, Gangwei F, Chengguo Z (2011) Underground pressure characteristics analysis in back-gully mining of shallow coal seam under a bedrock gully slope. Mining Science and Technology (China) 21:23-27. doi:https://doi.org/10.1016/j.mstc.2010.12.002
Yang J-H, Yu X, Yang Y, Yang Z-Q (2018a) Physical simulation and theoretical evolution for ground fissures triggered by underground coal mining. Plos one 13:e0192886.
Yang J-H, Yu X, Yang Y, Yang Z-Q (2018b) Physical simulation and theoretical evolution for ground fissures triggered by underground coal mining. PLoS ONE 13:1-30. doi:10.1371/journal.pone.0192886
Yang X, Wen G, Dai L, Sun H, Li X (2019) Ground Subsidence and Surface Cracks Evolution from Shallow-Buried Close-Distance Multi-seam Mining: A Case Study in Bulianta Coal Mine. Rock Mechanics and Rock Engineering 52:2835-2852. doi:10.1007/s00603-018-1726-4
Zhang D, Fan G, Ma L, Wang X (2011) Aquifer protection during longwall mining of shallow coal seams: A case study in the Shendong Coalfield of China. International Journal of Coal Geology 86:190-196. doi:https://doi.org/10.1016/j.coal.2011.01.006
Zhang J, Wang Z, Song Z (2020) Numerical study on movement of dynamic strata in combined open-pit and underground mining based on similar material simulation experiment. Arabian Journal of Geosciences 13:1-15.
Zhao K, Xu N, Mei G, Tian H (2016) Predicting the distribution of ground fissures and water-conducted fissures induced by coal mining: a case study. SpringerPlus 5:1-23.
Zhou CS, Zheng XQ, Zheng LY, Wei XO (2011) A study on the formation mechanism and preventive measures of coal-mining ground fissures in the south-west of Pingyao. Applied Mechanics and Materials. Trans Tech Publ. pp 1341-1344
Zhu G, Wu X, Yu S, Qian C, Dong Y, Zhang C, Wu C (2018a) Surface Water Control for Mining Thick, Relatively Shallow Coal Seams in the Loess Area of Western China. Mine Water and the Environment 37:442-455. doi:10.1007/s10230-018-0517-1
Zhu H, He F, Zhang S, Yang Z (2018b) An integrated treatment technology for ground fissures of shallow coal seam mining in the mountainous area of southwestern China: a typical case study. Gospodarka Surowcami Mineralnymi 34.

Figures

Lithology	Layer thickness /m
Aeolian sand	7
Red clay	5
Mudstone	2
Fine-grained sandstone	10
Siltstone	2
Fine-grained sandstone	2
Siltstone	1
Fine-grained sandstone	7
3-1 coal	3
Fine-grained sandstone	4
Mudstone	10
Siltstone	23
Siltstone	3
4-2 coal	4
Fine-grained sandstone	2

Figure 1

Experimental model

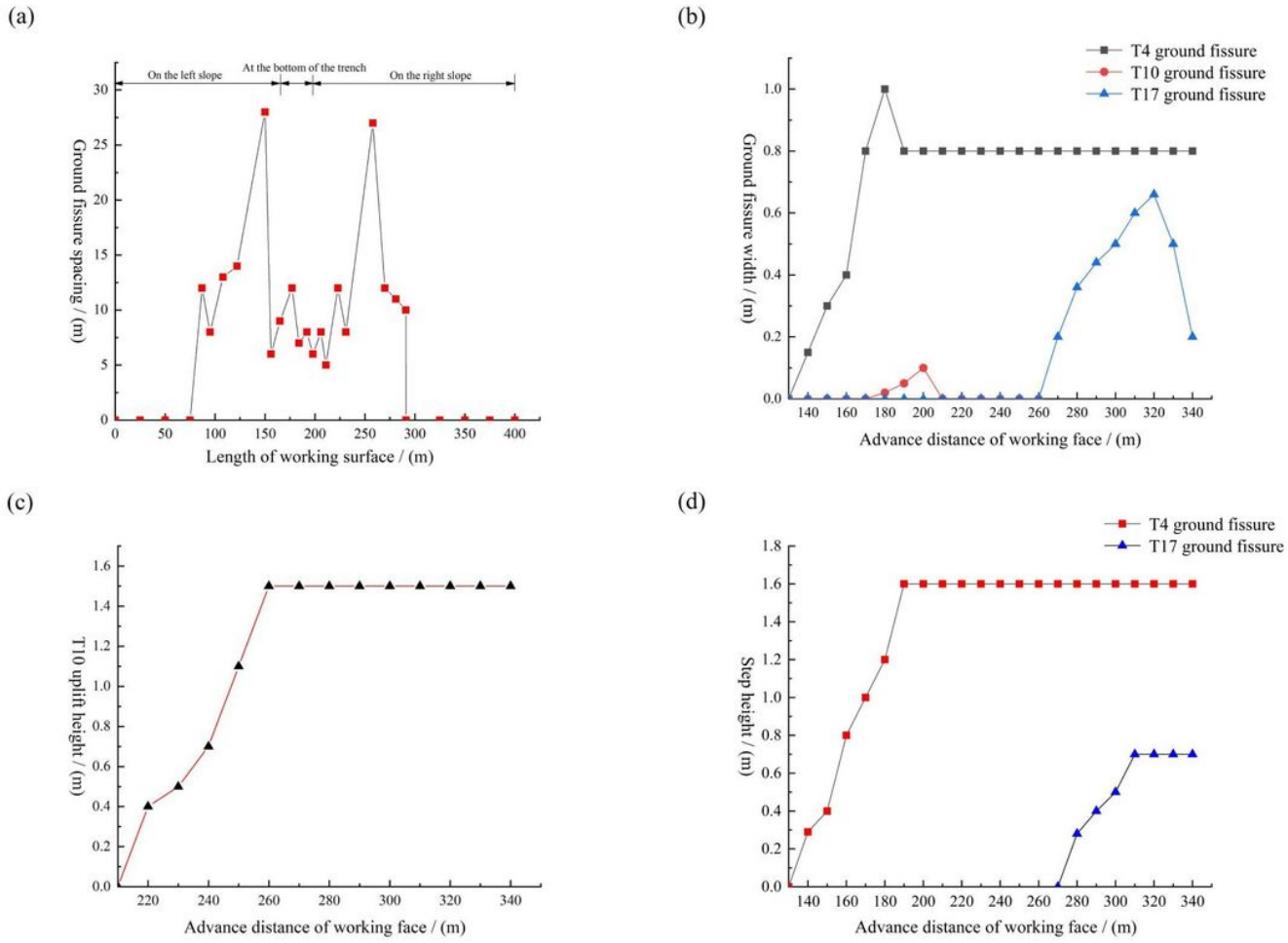

Figure 2

Dynamic development process of ground fissures : a distribution map of ground fissure spacing b, b dynamic width of ground fissure, c T10 uplift height chart, d T4 and T17 step height

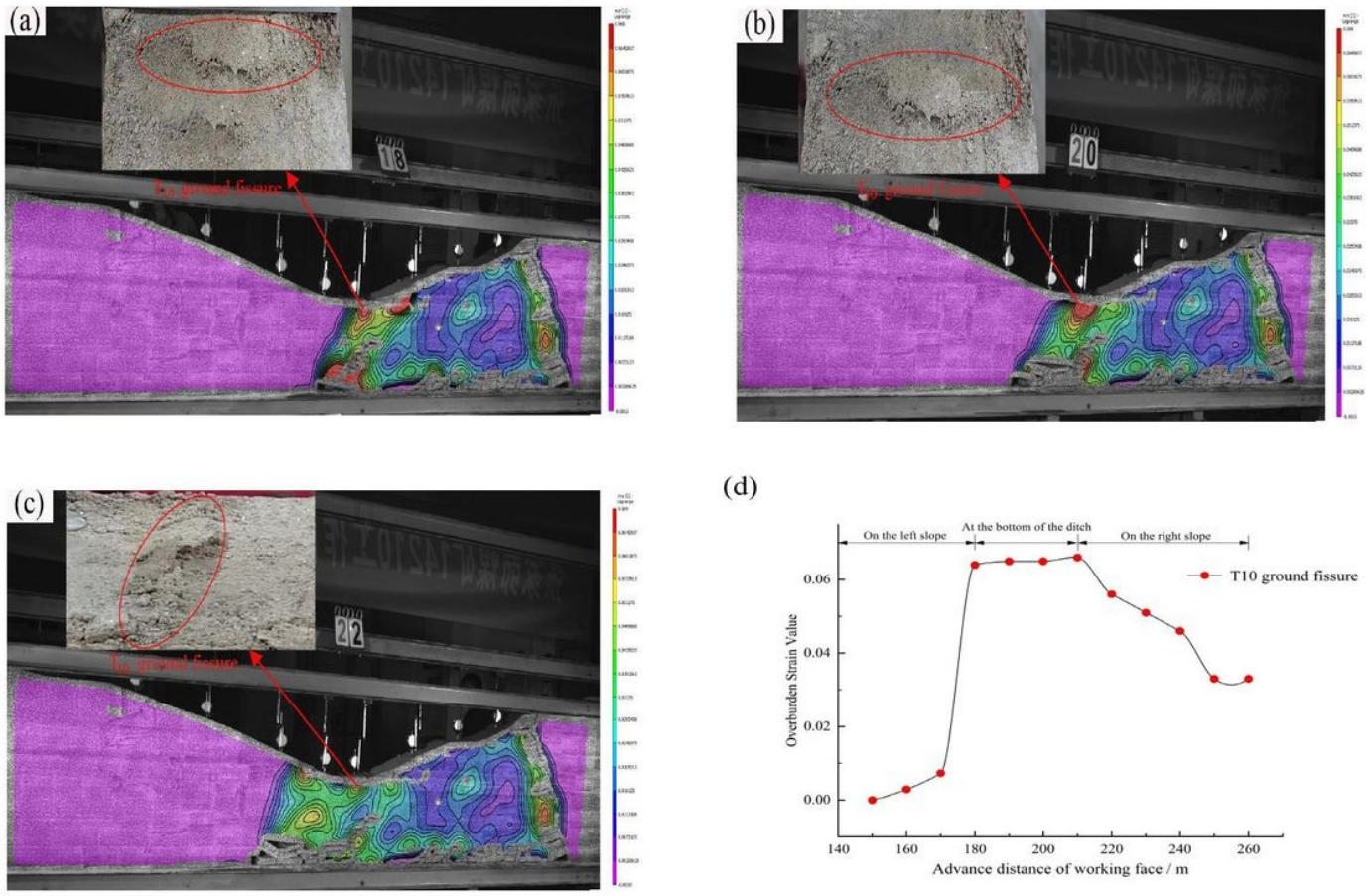

Figure 3

T10 ground fissure shape and underlying overburden strain : a working face advancing 180 m , b working face advancing 200 m , c working face advancing 220 m , d underlying overburden strain

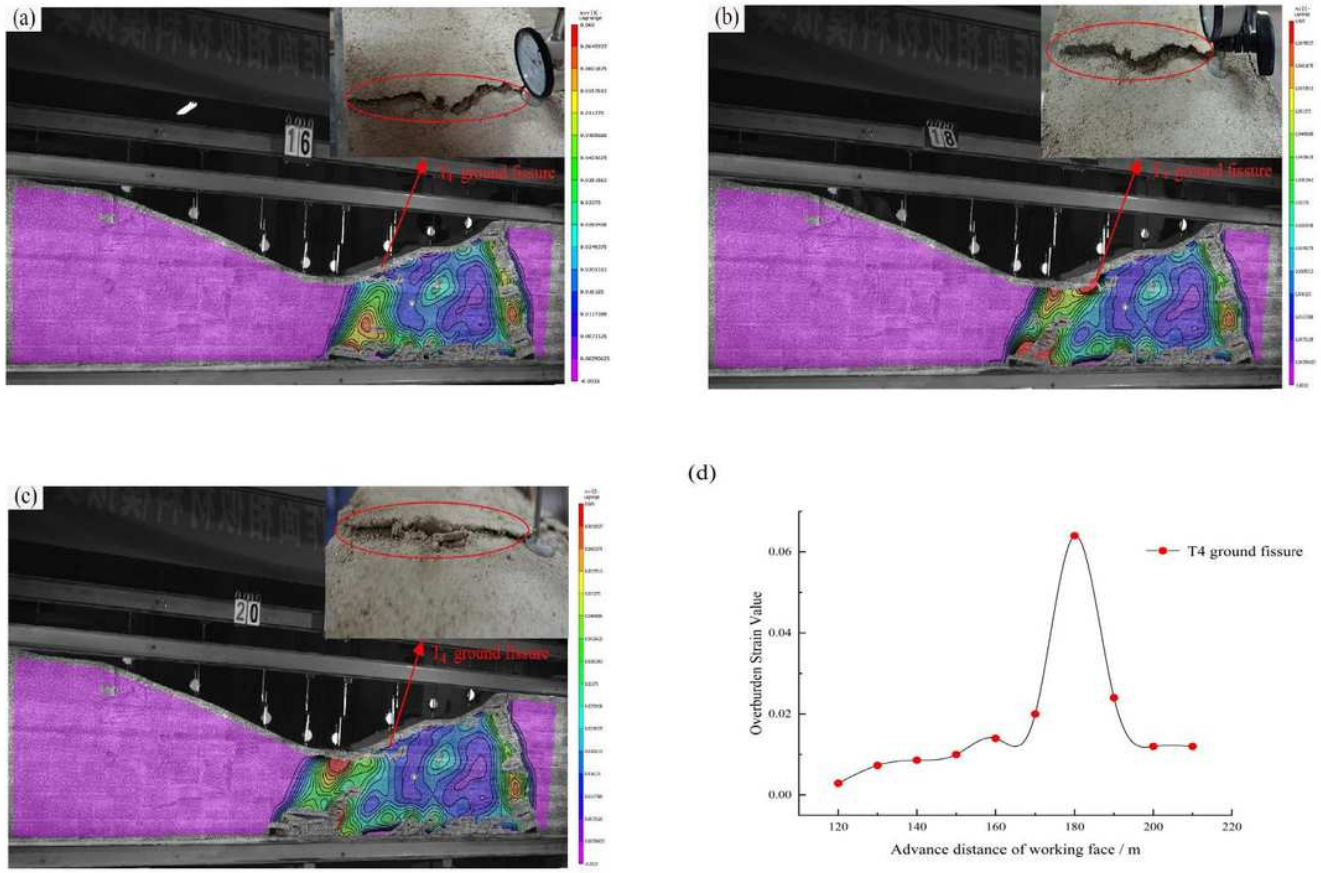

Figure 4

T4 ground fissure shape and underlying overburden strain a working face advancing 160 m , b working face advancing 180 m , c working face advancing 200 m , d underlying overburden strain

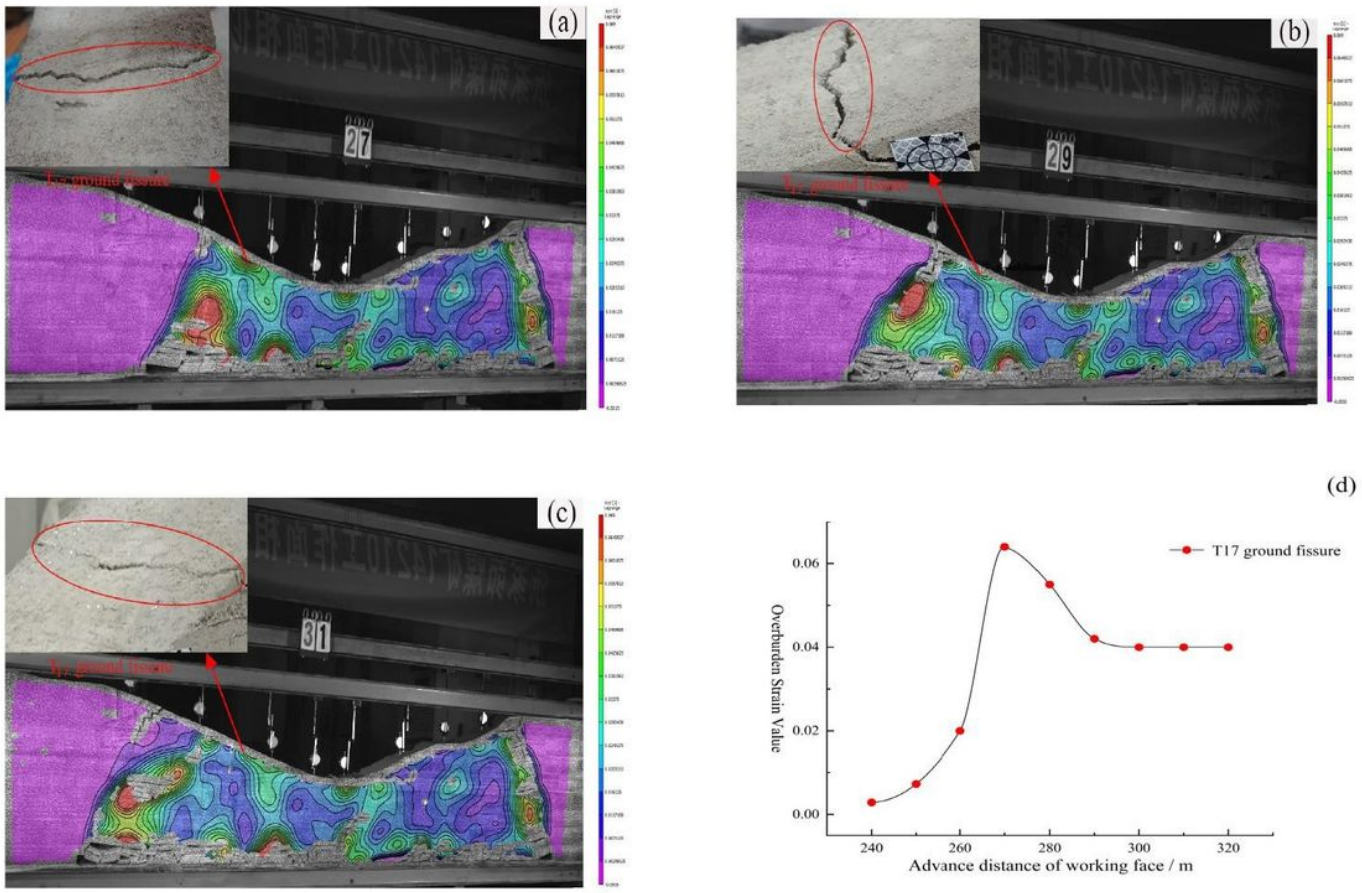

Figure 5

T17 strain variation process of the underlying overburden : a working face advancing 270 m , b working face advancing 290 m , c working face advancing 310 m , d underlying overburden strain

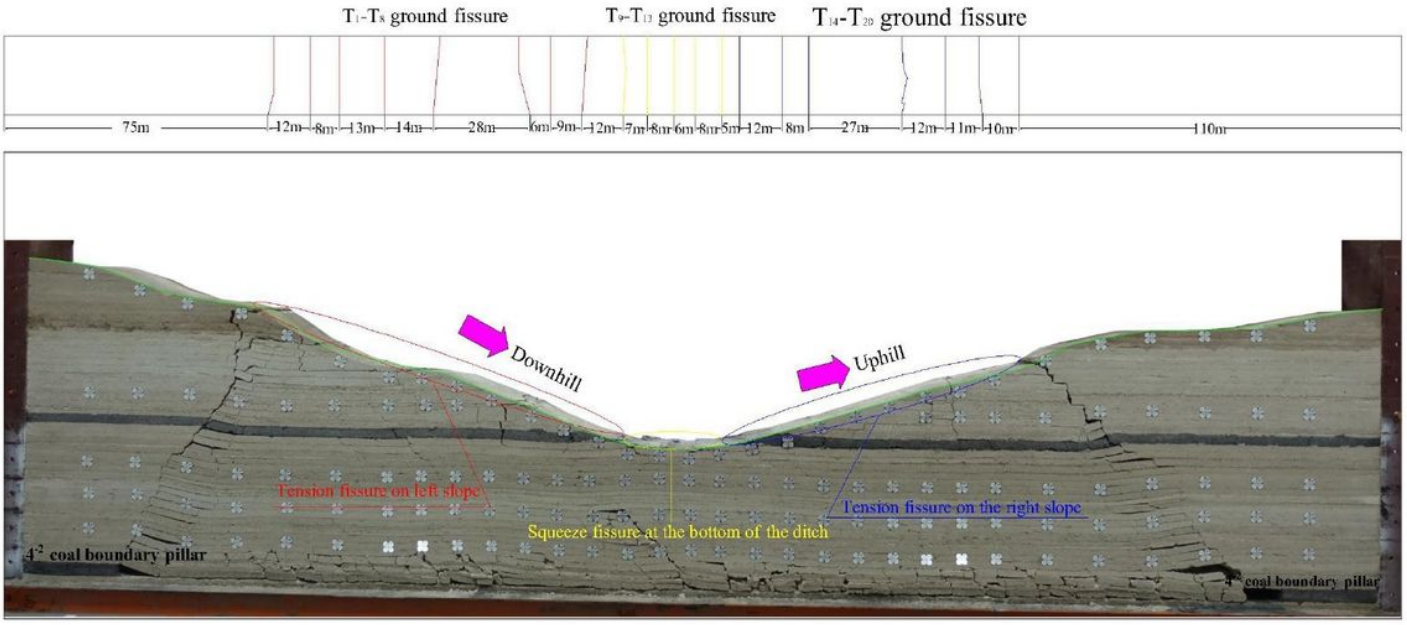

Figure 6

Ground fissures partition diagram